ADVANCED FUNCTIONAL MATERIALS
www.afm-journal.de

Adhesion of Catechol-Functionalized Linear-Dendritic Block Copolymers: Dendritic Effect, Self-Assembly, and Bioadhesion

Alexandre Lancelot, Mitchell E. Meger, Enrique Guerreiro Gómez, Teresa Sierra, and Jonathan J. Wilker*

Inspired by mussels protein adhesives, two series of catechol-functionalized Linear-Dendritic Block Copolymer (LDBC) adhesives are synthesized. They show lap shear adhesion strength as high as 7 MPa on aluminum substrates and adhesion up to 3 kPa on porcine skin. These water-soluble LDBCs are composed of i) either poly(ethylene glycol) (PEG) or poly(ethylene glycol)-poly(propylene glycol)-poly(ethylene glycol) triblock copolymer (Pluronic F-127) as linear polymers, ii) Bis-MPA dendrons of generation 0, 1, and 2 as dendritic parts, and iii) 2, 4, or 8 terminal catechol moieties. A LDBCs generation comparative test on aluminum reveals a clear dendritic effect: the LDBCs of second generation display higher adhesion than the LDBCs of first generation that also display higher adhesion than the LDBCs of generation 0 for both series, assessing thus a positive dendritic effect in adhesion. Second, a comparative study is carried out between the LDBCs based on PEG and the ones based on Pluronic. The ability of the Pluronic LDBCs to self-assemble in water appears to reduce adhesion when applied on aluminum whereas it is essential to obtain adhesion on porcine skin, thanks to the formation of hydrogels, as observed by the vial inversion technique and electron microscopy.

1. Introduction

Marine mussels can firmly stick on a large variety of substrates and under different environmental conditions. They have developed adhesives, named as mussel foot proteins (Mfps), to anchor onto the sea floor and make colonies (**Figure 1A**). These proteins contain 3,4-dihydroxyphenylalanine, or DOPA which is the main promoter of surface adhesion. DOPA presents a pending catechol moiety that favors both the adhesion and the cohesion of the Mfps.[1–3] In particular, catechol groups can foster strong adhesive interactions with the substrates via H-bonding, π–π stacking and metal chelation as well as covalent bonding through amine or thiol couplings. Moreover, catechols can associate with themselves via, again, H-bonding, π–π stacking and metal chelation as well as oxidative couplings forming crosslinked bridges.[4–6] Following Nature's insights, catechol-containing monomers have been copolymerized with acrylate,[7] glycidyl methacrylate,[8] styrene,[9] lactic acid,[10] and acrylic acid-butyl acrylate[11] among many others to prepare biomimetic adhesive polymers (Figure 1A).[12,13] Many systems show adhesive properties for both dry and underwater conditions. Hence, catechol-containing polystyrene, aka poly(vinylcatechol-styrene), showed underwater adhesion up to 3 MPa on aluminum substrates.[14,15] Catechol-containing polyvinylpyrrolidone displayed underwater adhesion up to 1.4 MPa when applied onto glass.[16] Catechol-containing sebacic acid-based polyester showed underwater adhesion ranging between 0.4 and 0.7 MPa on glass, aluminum and plastic substrates.[17]

A. Lancelot, E. Guerreiro Gómez, T. Sierra
Instituto de Nanociencia y Materiales de Aragón (INMA)
CSIC-Universidad de Zaragoza
Zaragoza 50009, Spain
E-mail: a.lancelot@unizar.es

The ORCID identification number(s) for the author(s) of this article can be found under https://doi.org/10.1002/adfm.202413398

DOI: 10.1002/adfm.202413398

A. Lancelot, E. Guerreiro Gómez, T. Sierra
Departamento de Química Orgánica
Facultad de Ciencias
Universidad de Zaragoza
Zaragoza 50009, Spain

A. Lancelot, M. E. Meger, J. J. Wilker
James Tarpo Jr. and Margaret Tarpo Department of Chemistry
Purdue University
560 Oval Drive, West Lafayette, IN 47907-2084, USA

J. J. Wilker
School of Materials Engineering
Purdue University
701 W. Stadium Avenue, West Lafayette, IN 47907-2045, USA

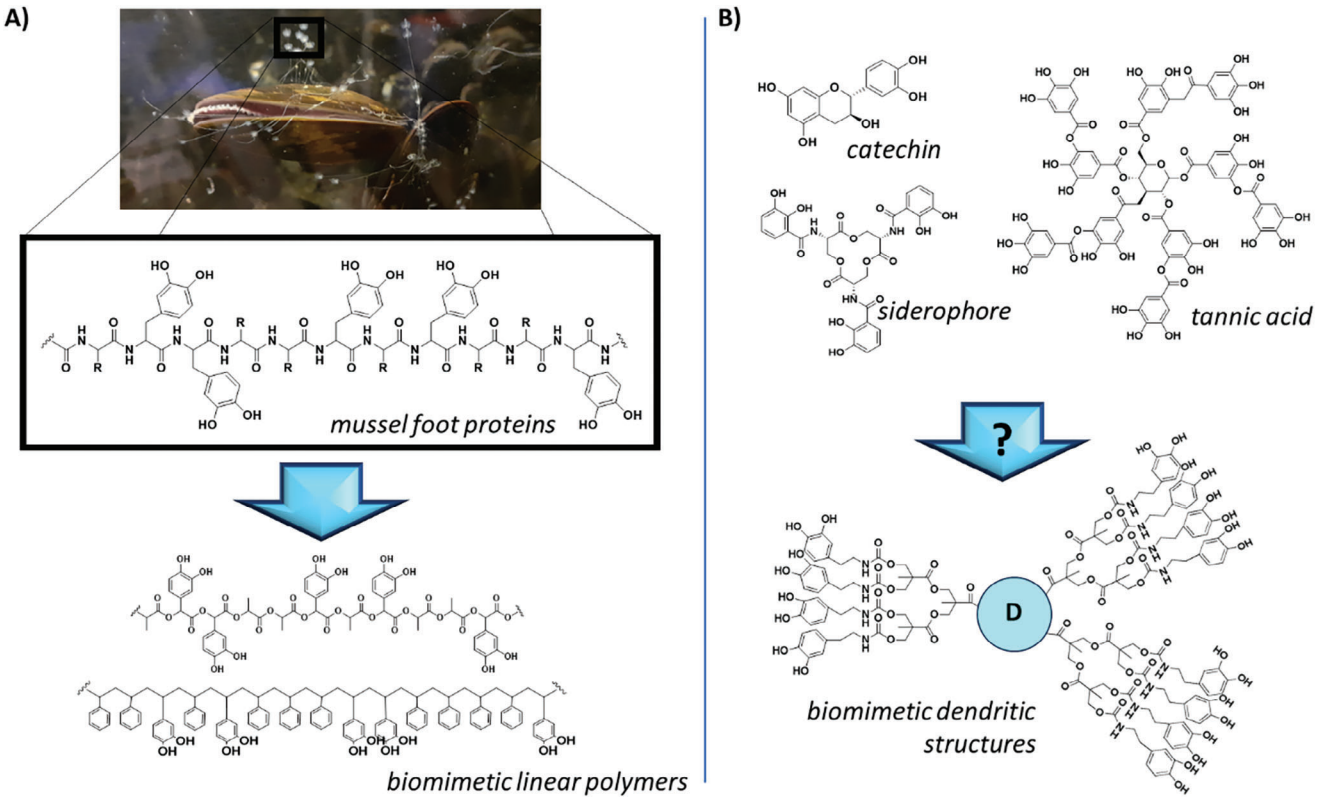

Figure 1. A) Chemical representation of mussel foot proteins inspiring catechol-containing biomimetic linear polymers[9,10] and B) Representations of catechin, siderophore and tannic acid that may inspire catechol-containing biomimetic dendritic derivatives.

Catechol groups are also found in other naturally occurring compounds such as catechin, tannic acid and siderophores (Figure 1B). In contrast with the Mfps, these molecules contain catechol moieties packed together within a more dense and rounded shape, which helps their function: preventing oxidation for catechin and transporting iron for siderophores. Similarly, dendrimers are a specific class of hyperbranched macromolecules that also adopt a globular architecture and present a high number of functional groups in a close proximity.[19–21] Moreover, these functional groups may behave synergistically promoting enhanced properties.[22–25] This so called dendritic effect was first observed in catalysis by Ford et al., in which the dendritic structure allowed an increase of the catalytic activity that was not proportional to the number of catalytic centers.[26] The dendritic effect was also leveraged in biomedical applications and sensors where it fostered multivalent and cooperative interactions between the receptors and the ligands increasing their affinity.[27–29] To date, few studies have explored the properties of catechol-functionalized dendrimers. Adhesive coatings were prepared using a polyglycerol dendritic core with catechols and amines,[30] and a catechol-functionalized polyethylenimine (PEI) was synthesized to develop antibacterial coatings.[31] In another study, a stimuli-responsive adhesive was obtained using a catechol-functionalized polyamidoamine (PAMAM) dendrimer, which showed adhesion up to 50 kPa on glass substrates.[32] In the particular case of bioadhesion, a 4-arm dendritic-like architecture with terminal catechols displayed adhesion when used on biological substrates[33] and a linear-dendritic block copolymer was used as an additive within a hydrogel formulation based on chitosan and carboxymethyl cellulose improving the hydrogel adhesion during ex vivo and in vivo experiments.[34] Also, a linear-dendritic block copolymer was reported, which presented intrinsic antibacterial properties and, after UV-curing, could adhere onto a patch developed for bone fixation surgery.[35] These recent studies confirmed the interest of developing novel linear-dendritic materials for adhesion purposes in general and especially, biological adhesion.

Hence, in this work, we embarked upon the synthesis and a complete study of the adhesive properties of two series of three novel biomimetic catechol-containing Linear-Dendritic Block Copolymers (catechol-LDBCs) bearing dendrons of generation 0, 1, and 2 (**Figure 2**). LDBCs have displayed interesting properties at the junction between the linear polymers and the dendrimers. As linear polymers, they are polydisperse macromolecules obtained through relatively simple synthetic steps and purifications. As dendrimers, they possess a defined and elevated density of accessible terminal groups, ready to be modified and to confer new properties to the macromolecules.[36] They avoid a tedious synthesis, which is crucial to develop new adhesives, while granting an easy and controllable functionalization to develop new materials. In this work, the LDBCs were designed as follows: i) a linear polymer, being either polyethylene glycol (PEG) or Pluronic F-127 (Plu), which is a triblock copolymer composed of polyethylene glycol – polypropylene glycol – polyethylene glycol, ii) modified at their edges with 2,2-bis(hydroxymethyl)propionic acid (Bis-MPA) dendritic parts and iii) functionalized with

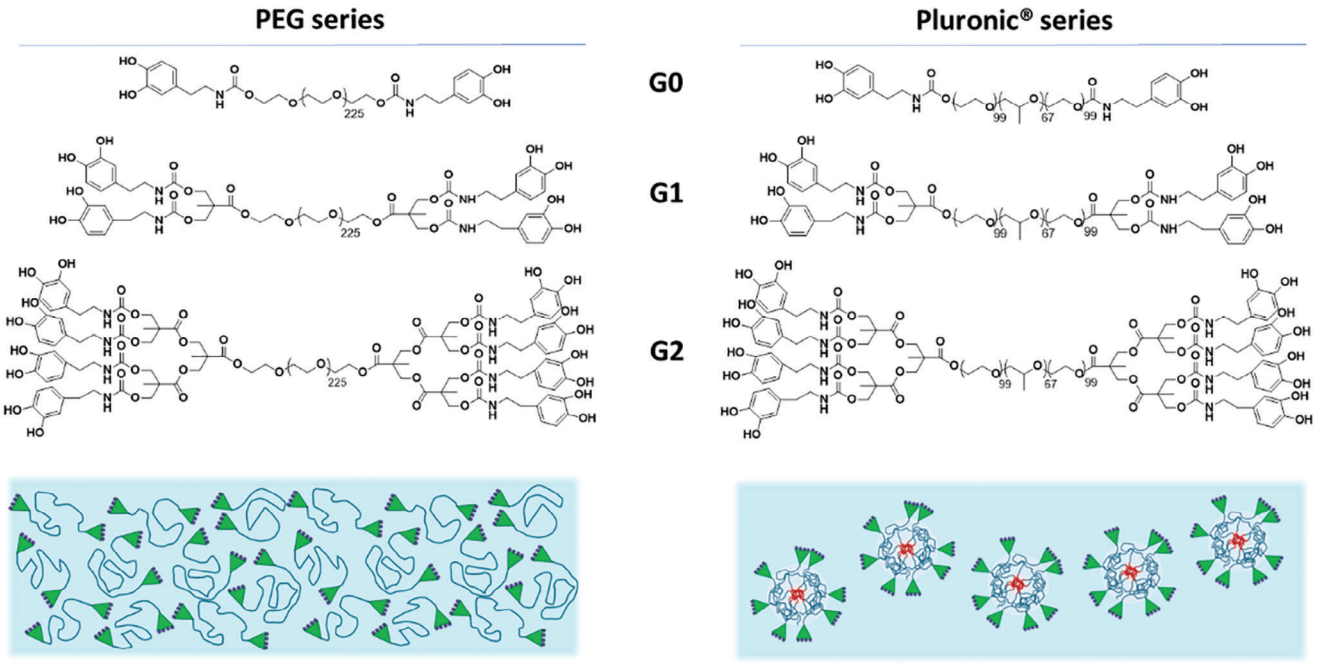

Figure 2. Chemical structures of the two series of the biomimetic catechol-LDBCs of generation 0, 1, and 2, (G0, G1, G2) and their proposed conformation when dissolved in water.

catechol moieties. Their synthesis will be discussed in the first part of the article.

Next, the influence of the LDBCs structural design upon adhesion was assessed. Indeed, it must be noticed that both linear polymers, PEG and Pluronic, have already been functionalized with catechol moieties at their end, showing good adhesion on porcine skin when used into several hydrogel mixtures, with adhesion values of 30 kPa[37] and up to 95 kPa[38] for PEG-based derivatives and 7 kPa[39] for a Pluronic-based derivative. In the present work, the insertion of the dendritic parts between the linear polymer and the terminal catechols allowed to increase the local density of terminal catechol moieties, seeking for adhesive synergy through the dendritic effect. The influence of such structural changes upon adhesion was studied by performing adhesion assays on aluminum. Next, the use of two different linear polymers brings substantial differences in the water solvation of both types of macromolecules. Whereas PEGs are fully hydrophilic polymers and tend to adopt random Gaussian coil conformations in water, typical of polymer chains in good solvent conditions,[40] Pluronic F-127 is an amphiphilic block-copolymer, which self-assembles in water forming micelles and hydrogels[41] (Figure 2). The influence of the difference in water solvatation of the catechol-LDBCs upon adhesion was studied by performing adhesion assays on aluminum and on porcine skin.

2. Results and Discussion

2.1. Synthesis

The six catechol-functionalized LDBCs presented hereby contained either PEG (MW 10 000 Da) or Pluronic F-127 (MW 12 000 Da) as linear polymers. Both linear polymers have molecular weights close to the one of the mussel foot proteins, i.e Mfp 5,[3] and fall within the MW range of previously published dendritic derivatives (from MW 2 to 48 Da).[30–35,37–39] PEG and Pluronic F-127 were chosen with close MWs to avoid significant influence of the MW upon the adhesion assays. Their synthesis (**Figure 3**) started growing Bis-MPA dendrons on the two extremities of each linear polymers following previously published reports.[42,43] It consisted of an esterification reaction using benzyl-protected anhydride derived from 2,2-bis(hydroxymethyl)propionic acid followed by the benzyl cleavage via hydrogenolysis. After, in order to incorporate the catechol functional group, each LDBC, G0, G1, and G2, displaying terminal hydroxyl groups, were first activated with p-nitrophenol chloroformate, and then allowed to react with dopamine forming a carbamate link between the dendritic part and the catechols.

According to this procedure, and thanks to the insolubility in diethyl ether of the two linear polymers, i.e. PEG and Pluronic F-127, only precipitations were required to obtain the final catechol-LDBCs. Thus, a relatively easy synthesis, on a 10–15 g batch scale, could be implemented without requiring tedious purifications while showing relatively good yields (**Table 1**).

The correct obtention of the catechol-LDBCs was confirmed by Fourier transform infrared (FTIR) spectroscopy, mass spectroscopy (MS), size exclusion chromatography (SEC) and proton nuclear magnetic resonance (^{1}H NMR). First, in the FTIR spectra, (Figure S4, Supporting Information), peaks between 1714 and 1724 cm^{-1} corresponding to the stretching of the carbonyl bonds were observed, attesting the presence of ester and carbamate groups. Second, MS analysis showed a broad distribution of peaks with maximum at ca. 11 kDa and ca. 13 kDa for unmodified PEG and Pluronic respectively. This maximum peak value increased after both, the growing of the Bis-MPA dendron and the

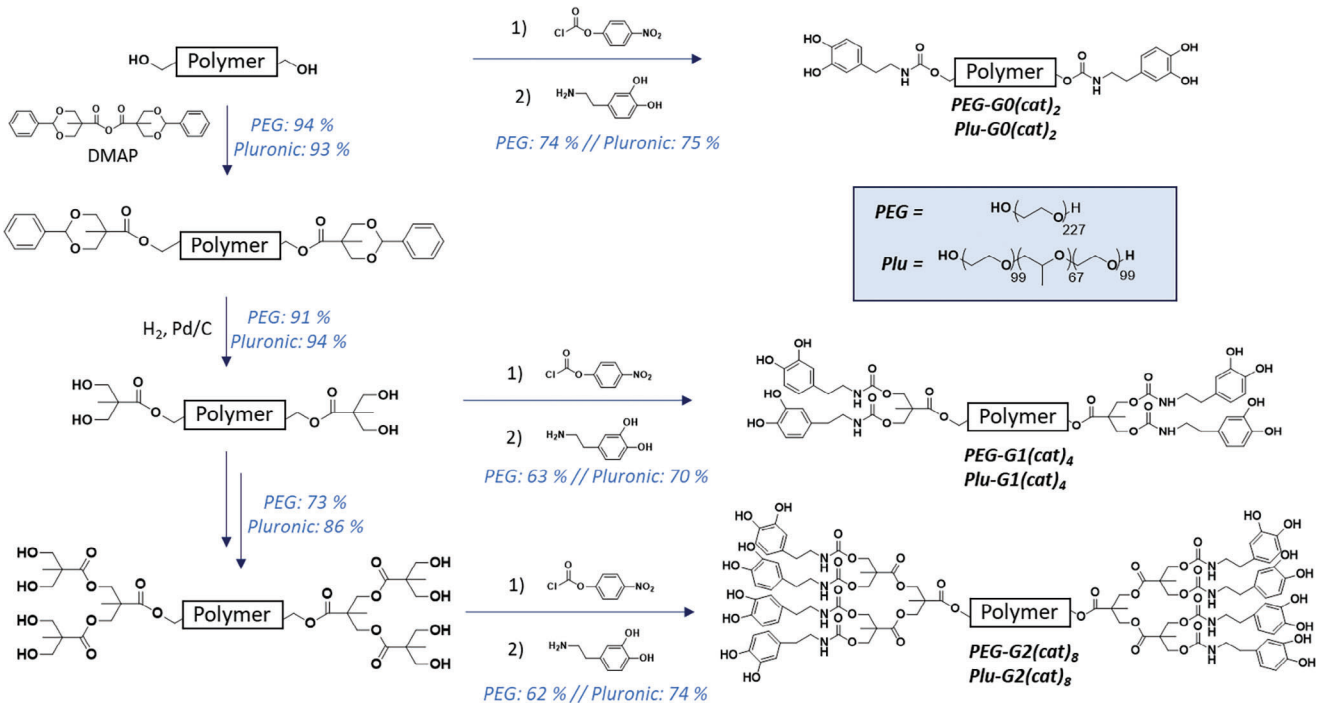

Figure 3. Synthesis scheme of the six biomimetic catechol-LDBCs with linear PEG or Pluronic F-127 and Bis-MPA dendrons of generation 0, 1, and 2 bearing 2, 4, and 8 catechol moieties respectively.

functionalization with catechol moieties. The same observation was made in SEC, where the relative measured molecular weight of the catechol-LDBCs increased with the generation (Figure S4 and Table S1, Supporting Information).

Third, in the ^{1}H NMR spectra (**Figure 4**; Figures S5 and S6, Supporting Information), the signals corresponding to the methylene groups of the polymers (blue label) were observed as a large peak ≈3.5 ppm. An additional peak corresponding to the signal of the methyl group was observed ≈1.2 ppm in the case of the Pluronic derivatives. The signals corresponding to the protons of the dendritic part (green label) were observed around 1.2 ppm and between 4.0 and 4.5 ppm. In the same area, the signal corresponding to the last methylene group localized at the extremities of the linear PEG or Pluronic was observed too, as evidenced by ^{1}H-^{1}H COSY experiments (Figure S7, Supporting Information). The signals corresponding to the protons belonging to the dopamine (red label) appeared as follows: 2.6 and 3.2 ppm for the methylene groups, 5.7 ppm for the carbamate proton, between 6.5 and 6.7 ppm for the aryl protons and the phenolic protons were seen as broad peaks ≈7.3 ppm.

Furthermore, by comparing, the relative peak intensity of the signals at 4.2 ppm, corresponding to both the dendritic part and the linear polymer, with the intensity of the peak at 2.6 ppm corresponding to the dopamine (labeled with a star in Figure 4), the degree of catechol functionalization was estimated for PEG/Plu-G1(cat)$_4$ and PEG/Plu-G2(cat)$_8$. Hence, good functionalization degrees were determined with values ranging from 78 to 98% (Table 1 and Supporting Information-1.3: Degree of catechol functionalization using ^{1}H NMR). Such estimations were strengthened by carrying out the Waite and Benedict spectroscopic DOPA assay.[44] In contrast to ^{1}H NMR spectroscopy, this assay could be performed for all the catechol-LDBCs, determining similar degrees of catechol functionalization, ranging from 79 to 88% (Table 1 and Supporting Information-1.4 Degree of catechol functionalization according to the Waite and Benedict DOPA assay.). Thus, in every case and independently of the dendritic generation, high levels of catechol functionalization were

Table 1. Yield and catechol functionalization according to ^{1}H-NMR spectroscopy and the Waite and Benedict DOPA assay.

Generation	PEG-based LDBCs			Pluronic-based LDBCs		
	Global yield [%]	Catechol funct. [%]		Global yield (%)	Catechol funct. [%]	
		^{1}H NMR	W &B assay		^{1}H NMR	W &B assay
0	74	–	88	75	–	83
1	54	91	79	61	96	81
2	39	86	84	55	78	79

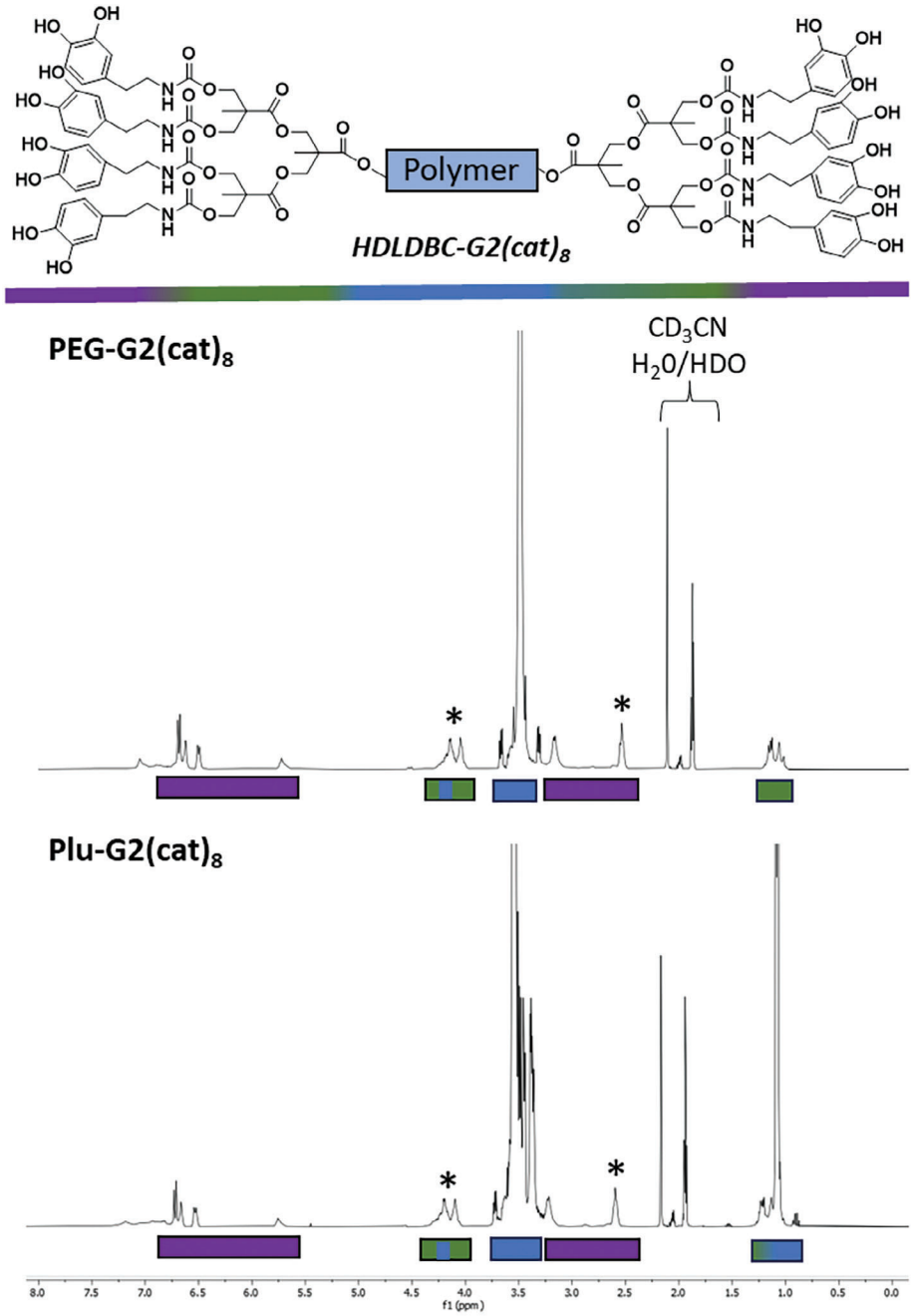

Figure 4. ^{1}H NMR spectra of PEG-G2(cat)$_8$ and Plu-G2(cat)$_8$ recorded in CD_3CN. H_2O and HDO signals were observed. The signals corresponding to the catechol part were labeled in purple, the ones corresponding to the Bis-MPA part in green and the ones corresponding to the polymer part in blue. The signals marked with a star were used to estimate the catechol functionalization.

achieved. The use of p-nitrophenyl chloroformate as an activating group for catechol functionalization of PEG and Pluronic yielded similar functionalization degrees than the previously described activation with N-hydroxysuccinimidyl ester.[37,39]

Hence, the hereby presented procedure allowed the relatively easy and efficient synthesis of six catechol-LDBCs, based on either PEG or Pluronic, and bearing 2, 4, or 8 terminal catechol moieties with good yields and high degree of catechol functionalization while using simple purification techniques.

2.2. Adhesion Studies on Aluminum – Dendritic Effect, Micellization and Fe$^{(III)}$ Addition

Before the adhesion assays, we checked the solubility of these novel catechol-LDBCs. Similarly to their constituting PEG and Pluronic F-127 linear polymer, they could be solubilized in a large variety of solvents including dichloromethane, tetrahydrofuran, ethanol, dimethyl sulfoxide or even water. For environmental and safety reasons and in order to reduce the use of organic solvents,

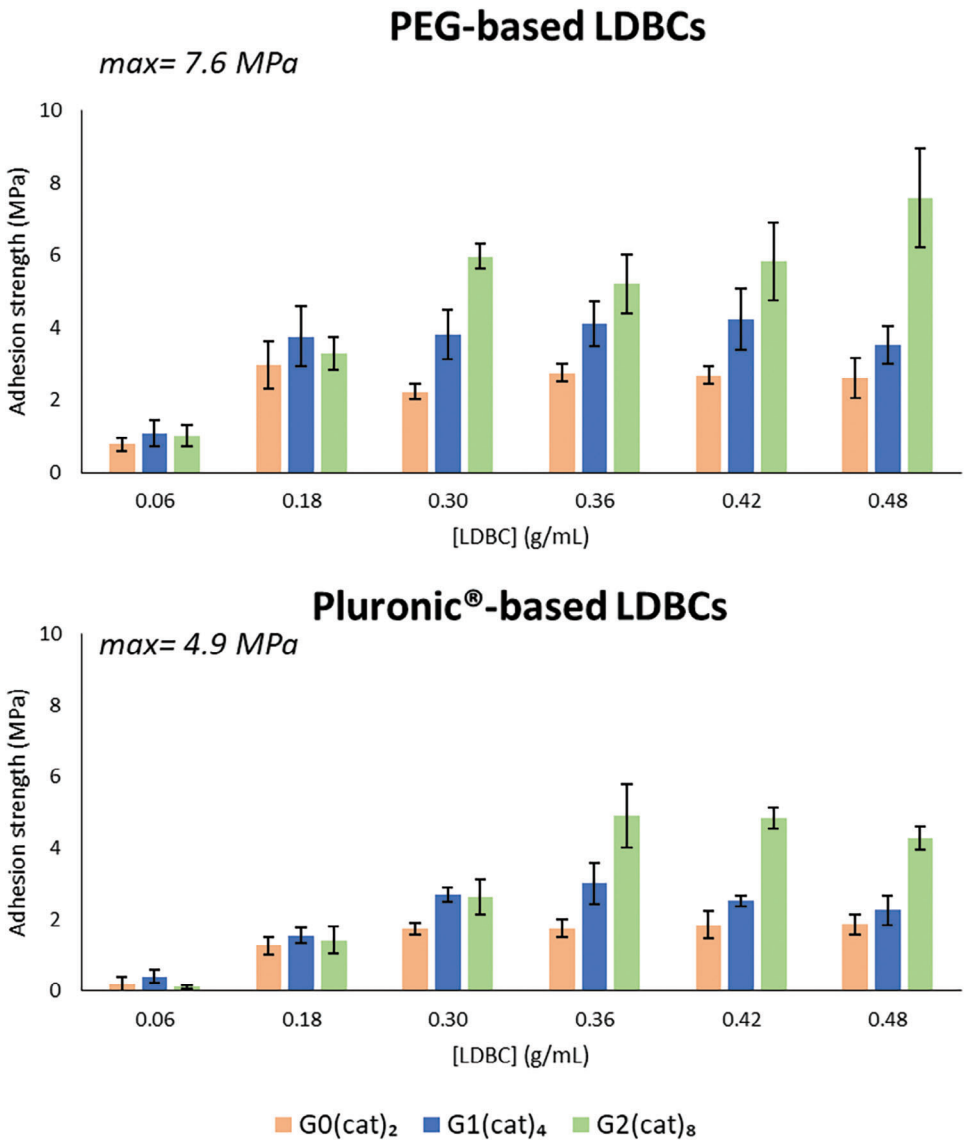

Figure 5. Adhesion strengths for PEG and Pluronic catechol-LDBC series at different concentrations in water on etched aluminum. Sample size (n = 5). Numerical values are gathered in the Tables S4 and S5 (Supporting Information).

distilled water was chosen as a solvent for the following adhesion tests. The obtention of homogeneous water dissolutions of all catechol-LDBCs was achieved by placing the mixtures of each solid catechol-LDBC with water in the fridge (4 °C) overnight. Pluronic derivatives are often more soluble in cold water and this dissolution technique was previously described.[43,45]

Then, the adhesion assay of the six catechol-LBDCs, dissolved in water at concentrations ranging from 0.06 to 0.48 g mL^{-1}, was conducted on etched aluminum substrates. All the samples were cured as followed: 1 h at room temperature to favor a good wetting of the substrates, followed by 22 h at 120 °C to evaporate the water, and then 1 h at room temperature to allow the samples to go back to room temperature before the assay. This curing procedure was adapted from previously used procedures in our laboratory that afforded repeatable and reproducible adhesion values.[9,10,15] After curing the adhesive, its adhesion strength was measured by performing lap shear strength experiments that consisted of moving up one of the two substrates while maintaining the second one in a fixed position. The force was applied parallelly to the adhesive and was continuously measured by the equipment until the adhesive break recording a strain versus stress curve. From the curve, the maximum force load applied to the adhesive (**Figure 5**) and the area under the curve were determined (Tables S3 and S4, Supporting Information).

First, the adhesion assays confirmed that all the catechol-LDBCs showed effective adhesion on aluminum with maximal adhesive forces up to 7 MPa for the PEG-based LDBCs and up to 5 MPa for the Pluronic-based LDBCs. The stress versus strain curves were typical of brittle adhesives, displaying a linear increase of the stress versus strain followed by a sharp decrease after reaching the maximum of adhesion (see Figures S10–S15, Supporting Information).[46] Cohesive failures,

Table 2. Adhesive strength of PEG-G2(cat)$_8$ and Plu-G2(cat)$_8$, previously published polymer adhesives and commercial adhesives.[1]In the cited references, adhesives were applied and were cured following different protocols before adhesion assays. [2]The commercial adhesives were applied on aluminum and were cured at room temperature following the manufacturer's recommendations.

Adhesive systems		Adhesion (MPa)
this work	PEG-G2(cat)$_8$	7.6 ± 1.4
	Plu-G2(cat)$_8$	4.7 ± 0.3
previously published works[1]	Catechol-containing polystyrene[9]	11.0 ± 0.5
	Catechol-containing poly lactic acid[10]	2.6 ± 0.4
	Catechol-containing sebacic acid-based polyester[17]	0.8 ± 0.2
	Catechol-containing poly(vinylpyrrolidone)[16]	0.7 ± 0.1
commercial adhesives[2]	Gorilla glue (polyurethane)	2.7 ± 0.2
	Super Glue (cyanoacrylate)	4.9 ± 0.5

i.e., breaking within the bulk of the adhesive, were observed. In similar conditions, unmodified PEG and Pluronic polymers, as well as PEG-G1(OH)$_4$ and PEG-G2(OH)$_8$ did not show any adhesion. Such result was not surprising since PEG and Pluronic are often used to limit molecular interactions and as antifouling agents.[47,48] However, the addition of the catechol groups transformed them into water-soluble adhesive macromolecules. The measured adhesive values were in the range of several commercial glues, like Gorilla glue or Super Glue, and other previously published polymer adhesives with pendant catechol moieties. Adhesion values of such systems are gathered in the **Table 2** for illustration. Nevertheless, a direct comparison between different adhesive systems maximal strength should be done carefully since they were applied and cured differently.

Second, for both series, it can be noticed that, in almost every case, the LDBCs of higher generation showed the strongest adhesion. The maximum of adhesion reached for each LDBC of the two series, PEG and Pluronic, increased with the LDBC generation (see **Table 3**). With PEG/Plu-G0(cat)$_2$ a maximum of adhesion ≈2–3 MPa was reached, whereas with PEG/Plu-G1(cat)$_4$ such adhesion maximum was higher, i.e., 3–4 MPa, and, finally, 5–8 MPa were reached with PEG/Plu-G2(cat)$_8$. Similarly, the areas under the curve also increased with the LDBCs generation, starting from 80 N.mm for PEG-G0(cat)$_2$ and going up to 520 N.mm for PEG-G2(cat)$_8$ (see Figure S16, Tables S4 and S5, Supporting Information). Accordingly, the LDBCs with the higher dendritic generation were able to overpass the overall adhesion limit observed for the LDBCs with a lower dendritic generation. For example, as for PEG-based LDBCs, PEG-G0(cat)$_2$ reached its maximum of adhesion at concentrations equal or higher than 0.18 g mL^{-1} (which corresponded to 35 µmol of catechol/mL) while PEG-G1(cat)$_4$ reached its maximum of adhesion at concentrations equal or higher than 0.36 g mL^{-1} (132 µmol of catechol/mL) and PEG-G2(cat)$_8$ reached its maximum of adhesion at concentration equal to 0.48 g mL^{-1} (317 µmol of catechol/mL). A similar trend was observed for Pluronic-based LDBCs. Thanks to the dendritic architecture, the local concentration of catechol moieties increased with the dendritic generation, allowing these moieties to work in synergy showing a higher adhesion threshold. This result confirmed the manifestation of a positive dendritic effect here, as it has been described for multidentate adhesive moieties that have shown enhanced adhesion.[49,50] Notwithstanding, this is the first time that a positive dendritic effect was observed for catechol-functionalized macromolecules with adhesive applications to our knowledge.

Table 3. Maximum adhesion strength values attained for each catechol-LDBC and the critical concentration required to reach this value. Sample size (n = 5).

Generation	PEG-based	Pluronic-based
PEG/Plu-G0(cat)$_2$	2.6 MPa when [c] ≥ 0.18 g mL^{-1}	1.8 MPa when [c] ≥ 0.30 g mL^{-1}
PEG/Plu-G1(cat)$_4$	4.0 MPa when [c] ≥ 0.36 g mL^{-1}	2.6 MPa when [c] ≥ 0.30 g mL^{-1}
PEG/Plu-G2(cat)$_8$	7.6 MPa when [c] ≥ 0.48 g mL^{-1}	4.7 MPa when [c] ≥ 0.36 g mL^{-1}

Third, PEG-based LDBCs showed higher adhesion strength than Pluronic-based LDBCs. Maximum strengths were equal to 7.6 MPa for PEG-G2(cat)$_8$ and 4.7 MPa for Plu-G2(cat)$_8$ at 0.48 g mL^{-1}. Such variation can be related to the distinct conformations adopted by the LDBCs when dissolved in water. Unlike PEG, Pluronic F-127 self-assembles in water forming micelles because of its amphiphilicity.[51] Pluronic-based LDBCs shared the same behavior and micelles with diameters ranging from 20[52] to 300 nm[53] have been previously described. An easy and standard assay to confirm the formation of micelles is the Nile Red solvatochromic assay. Nile Red is a dye that shows low fluorescence emission in a hydrophilic medium and high fluorescence emission in a lipophilic medium. When aggregates, like micelles, are formed in water Nile Red migrates into their inner part and exhibits high fluorescence.[54] In this study, the emission spectra of Nile Red for the Pluronic-based LDBCs and the PEG-based LDBCs were clearly different (**Figure 6A**), attesting the formation of micelles in the case of Pluronic-based LDBCs and their absence in the case of PEG-based LDBCs. The formation of micelles also affected the viscosity of the LDBCs aqueous dissolutions (Figure 6B). The viscosity of PEG-G2(cat)$_8$ and Plu-G2(cat)$_8$ dissolutions in water was measured at different shear rates and concentrations to evaluate the influence of the linear polymer upon viscosity. In all cases the dissolutions appeared as Newtonian fluids, which means that their viscosity was independent of the shear rate. However, Plu-G2(cat)$_8$ dissolutions appeared to be more viscous than the PEG-G2(cat)$_8$ dissolutions. For PEG-G2(cat)$_8$, the viscosity of the dissolutions increased

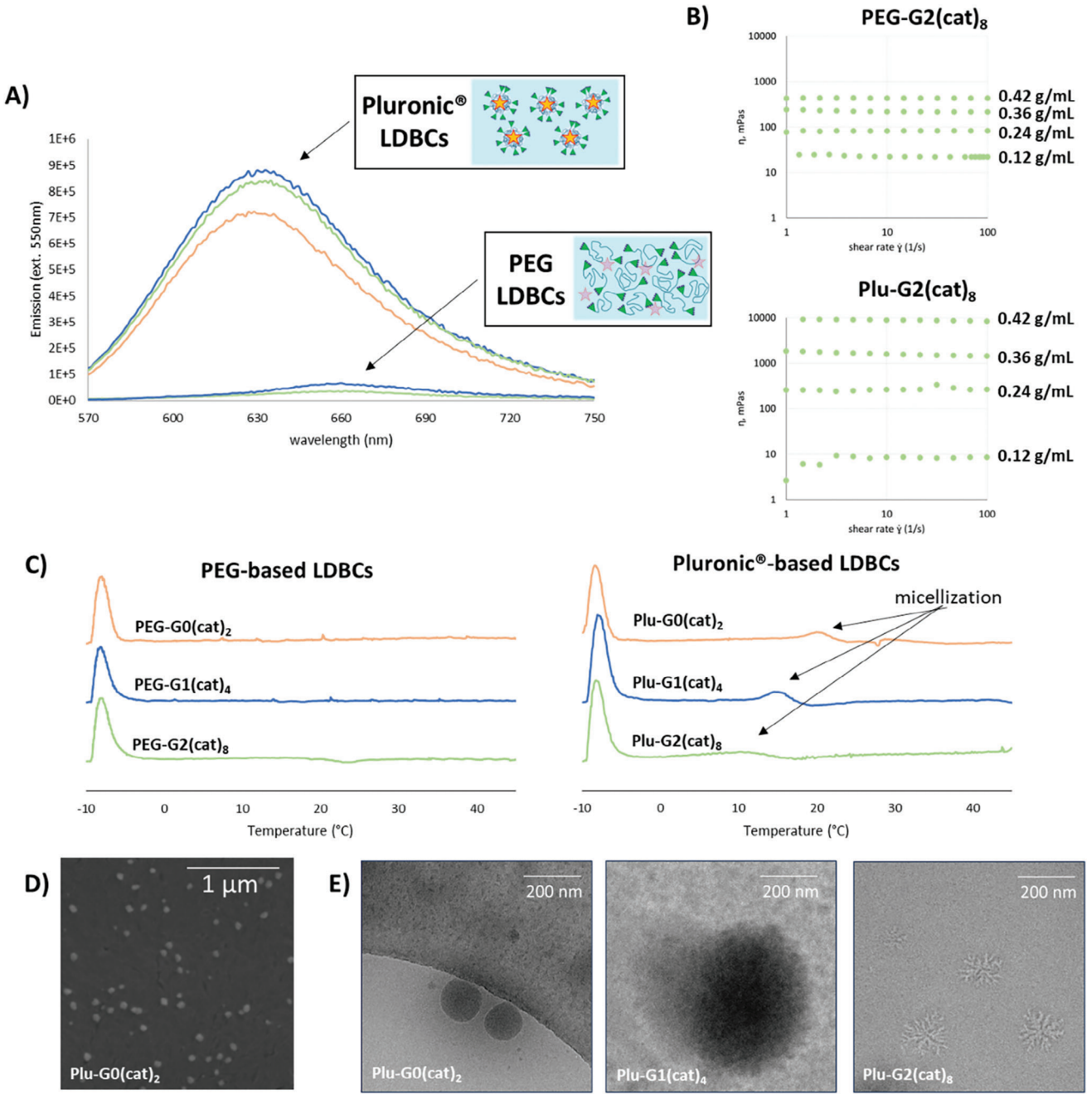

Figure 6. Pluronic-based LDBCs micellization in water. A) fluorescence spectra of Nile Red within PEG-based versus Pluronic-based LDBC solutions. B) viscosity curves of PEG-G2(cat)$_8$ and Plu-G2(cat)$_8$ in water. C) derivatives of the DSC curves of the Pluronic-based LDBCs in water. D) SEM image of the micelles formed by the Plu-G0(cat)$_2$ in water and E) cryoTEM images of the objects formed by Plu-G0(cat)$_2$, Plu-G1(cat)$_4$, and Plu-G2(cat)$_8$ in water.

linearly with the concentration and ranged between 22 and 428 mPas. On the other hand, for Plu-G2(cat)$_8$, the viscosity of the dissolutions ranged from 8 to 8700 mPas, and the increase in viscosity was no longer linear due to the presence of micelles.

To further characterize the micelles formed by the Pluronic-based LDBCs, the critical micellar concentrations (CMCs) and the critical micellar temperatures (CMTs) were determined. According to the Nile Red assay, the CMCs were ≈0.03 g mL^{-1} at 20 °C for the three Pluronic LDBCs (Figure S9, Supporting Information), which is similar to the values of unmodified Pluronic. The CMTs were observed as an enthalpic transition in differential scanning calorimetry experiments (Figure 6C).[55] Their value decreased while increasing the dendritic generation, being ≈21, 14, and 10 °C for Plu-G0(cat)$_2$, Plu-G1(cat)$_4$, and Plu-G2(cat)$_8$ respectively. Finally, the micelles formed by Plu-G0(cat)$_2$ were observed in Scanning Electron Microscopy (SEM) as spherical objects with diameters between 50 and 100 nm (Figure 6D). Cryogenic Transmission Electron Microscopy (cryoTEM) allowed to observe the

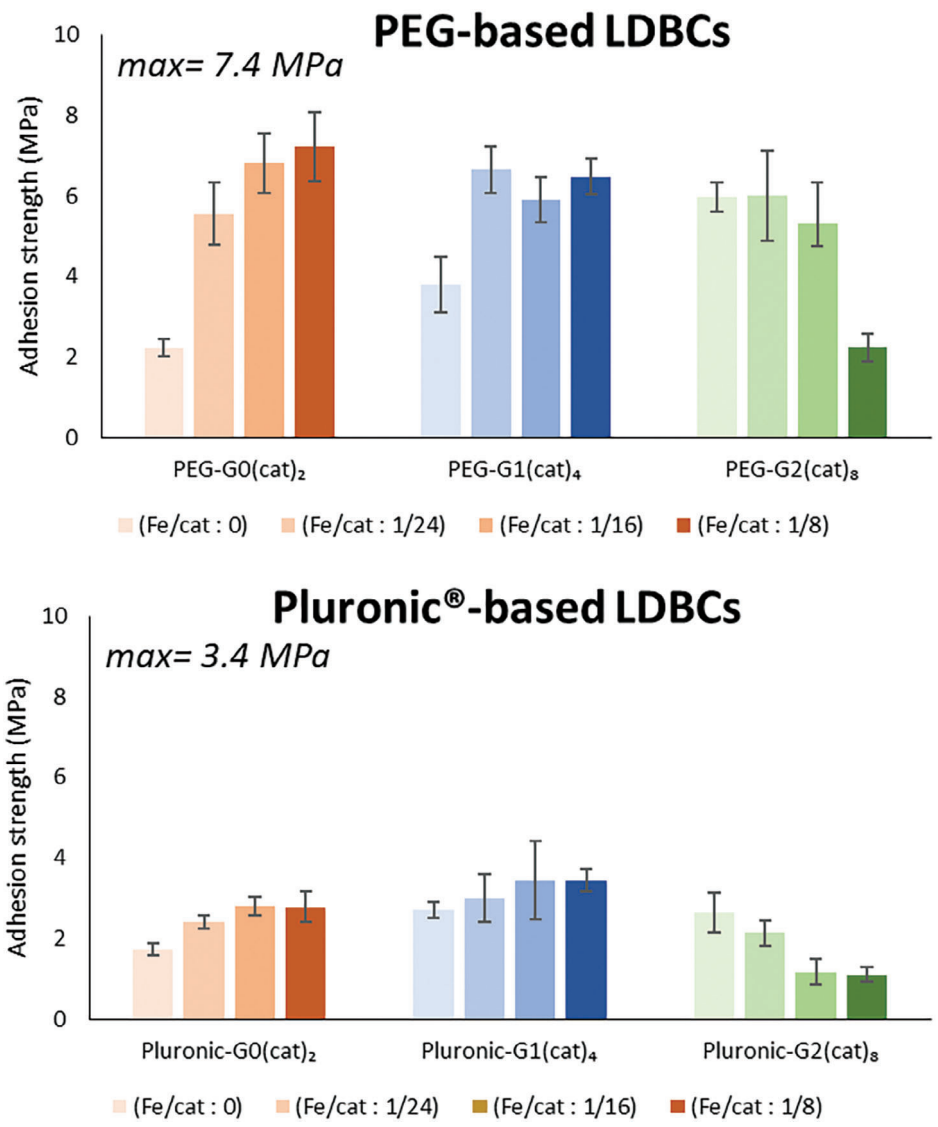

Figure 7. Adhesion strengths for PEG and Pluronic catechol-LDBC series at 0.3 g mL^{-1} in water on etched aluminum with different quantities of $Fe^{(III)}$: (Fe/cat in mol = 0, 1/24, 1/16, and 1/8). Sample size (n = 5). Numerical values are gathered in the Tables S6 and S7 (Supporting Information).

micelles in solution (Figure 6E,D). With this technique, the micelles formed by Plu-G0$(cat)_2$ appeared as slightly bigger spherical objects, with diameters ranging from 100 to 150 nm, due to the swelling of the hydrophilic corona of the micelles. The micelles formed by Plu-G1$(cat)_4$ were bigger with diameters ranging from 200 to 500 nm. Plu-G2$(cat)_8$ appeared as different objects, adopting the form of snowflakes with diameters ranging from 100 to 200 nm. Interestingly, the dendritic generation of the Pluronic-based LDBCs led to the formation of structures of different size and/or morphology.

Next, to continue to mimic the mussels behavior, $FeCl_3$ was added to all the LDBC adhesive formulations at different molar ratios (Fe/cat: 1/24, 1/16 and 1/8). Indeed, mussels can improve the mechanical properties of their natural Mfps adhesive using catechol-Fe interactions to promote internal crosslinking and enhance surface interactions.[56] In this specific study, assays were carried out at the fixed concentration of 0.3 g mL^{-1} (**Figure 7**). Here too, PEG-based LDBCs showed higher adhesion strengths than the Pluronic-based LDBCs. Adhesives remained brittle and the failure mode was not affected, remaining cohesive in nature.

For both series, adhesion improvement was visible for the derivatives with the smallest dendron generations, G0 and G1, in contrast to G2 derivatives that showed a loss of adhesive properties. Interestingly, within each series, and regardless of the central linear polymer, PEG/Plu-G0$(cat)_2$ showed the most dramatic rise in adhesion strength (**Table 4**). Particularly, after $Fe^{(III)}$ addition, PEG-G0$(cat)_2$ increased its adhesion by a factor of more than 3, while Plu-G0$(cat)_2$ showed an increase by a factor of 1.5. PEG/Plu-G1$(cat)_4$ displayed a more moderated increase and PEG/Plu-G2$(cat)_8$ showed a decrease of adhesion strength. These results might be explained by the different interactions between the $Fe^{(III)}$ cations and the catechol-LDBCs of different generations. One single $Fe^{(III)}$ cation might coordinate with up to three different catecholate units.[57] To form such complexes,

Table 4. Maximum adhesion strength values obtained for each catechol-LDBC with $Fe^{(III)}$ and the relative increase of adhesion when compared to the absence of $Fe^{(III)}$. $Fe^{(III)}$/cat ratios are given in mol. Sample size (n = 5).

Generation	PEG-based LDBCs		Pluronic-based LDBCs	
	no $Fe^{(III)}$	with $Fe^{(III)}$	no $Fe^{(III)}$	with $Fe^{(III)}$
PEG/Plu-G0$(cat)_2$	2.2 ± 0.2 MPa	7.2 ± 0.9 MPa at (1/8) ↑ 323% increase	1.7 ± 0.2 MPa	2.8 ± 0.4 MPa at (1/16) ↑ 61% increase
PEG/Plu-G1$(cat)_4$	3.8 ± 0.7 MPa	6.7 ± 0.6 MPa at (1/24) ↑ 170% increase	2.7 ± 0.2 MPa	3.4 ± 0.3 MPa at (1/16) ↑ 29% increase
PEG/Plu-G2$(cat)_8$	6.0 ± 0.4 MPa	2.2 ± 0.4 MPa at (1/18) ↓ 63% decrease	2.6 ± 0.5 MPa	1.1 ± 0.2 at (1/8) ↓ 58% decrease

$Fe^{(III)}$ and PEG/Plu-G0$(cat)_2$ needed to interact at the intermolecular level, joining up to 3 LDBCs together in one crosslinking point, reinforcing the cohesion of the adhesive. On the contrary, for PEG/Plu-G2$(cat)_8$, one single $Fe^{(III)}$ cation could be intramolecularly complexed by only one LDBC. The formation of such complexes hindered the intermolecular crosslinking responsible for the reinforcement of the adhesive cohesion and, in addition, utilized catechol residues that were no longer available for adhesion, thus explaining the observed decrease in adhesion. As an alternative to $Fe^{(III)}$, H_2O_2 was used as an oxidant to promote catechol-catechol crosslinking. However, no notable improved performance was found (see Supporting Information-2.3: Numerical data and graphs using HO· as a crosslinking agent).

In summary, the catechol-LDBCs hereby presented were able to show strong adhesion on aluminum substrates with interesting insights. First, a clear effect of the dendrimer generation was observed, confirming a positive dendritic effect for both PEG and Pluronic-based adhesive systems. Second, the central linear polymer also played a key role. By forming micelles in water, Pluronic-based LDBCs showed lower adhesion values than PEG-based LDBCs. Third, crosslinking could be induced by coordination with $Fe^{(III)}$, increasing the adhesion for PEG/Plu-G0$(cat)_2$ and PEG/Plu-G1$(cat)_4$.

2.3. Bioadhesion on Porcine Skin and Hydrogelation

Usually, LDBCs based on PEG or Pluronic and Bis-MPA have been implemented for biomedical applications.[58] They are known to be biocompatible and their degradation or elimination in vivo has also been established.[59] Mostly used in drug delivery, they were able to improve several drug bioavailabilities, pharmacokinetics and activities during in vitro and/or in vivo experiments while showing high cell viability.[60,61] Following that alluring biomedical direction, the bioadhesive properties of the present catechol-LDBCs have been examined. The bioadhesion assays were carried out using wet porcine skin as a model. For this assay, the catechol-LDBCs were dissolved in water at 0.8 g mL^{-1} before application. The adhesive formulations were cured for 24 h at 33 °C, i.e., skin temperature, within a humid chamber (**Figure 8**) and the adhesive strength was measured performing lap shear adhesion tests.

In this experiment, no adhesion was observed for the PEG-based LDBCs. At 33 °C, these adhesive formulations remained liquid, showing insufficient curing, even after 24 h. In contrast, all the Pluronic-based LDBCs showed effective adhesion on wet porcine skin. Values ranged between 2 and 3 KPa, with no significant influence of the generation, and adhesive failure mode in all cases. Such values were slightly higher than the one obtained for TISSEEL, a commercial fibrin sealant used in surgery (Figure 8B).

The differences in adhesion while comparing the PEG-based LDBCs with the Pluronic-based LDBCs were related to the self-assembly behavior of Pluronic F-127 in water. As depicted in Figure 6, the Pluronic-based LDBCs formed micelles in water at concentrations superior to 0.03 g mL^{-1} at 20 °C. At higher temperatures and concentrations, the formation of hydrogels was observed for those LDBCs using the vial inversion technique (**Figure 9A**). Interestingly, the critical gelation concentration (CGC) gently increased with the LDBCs generation,

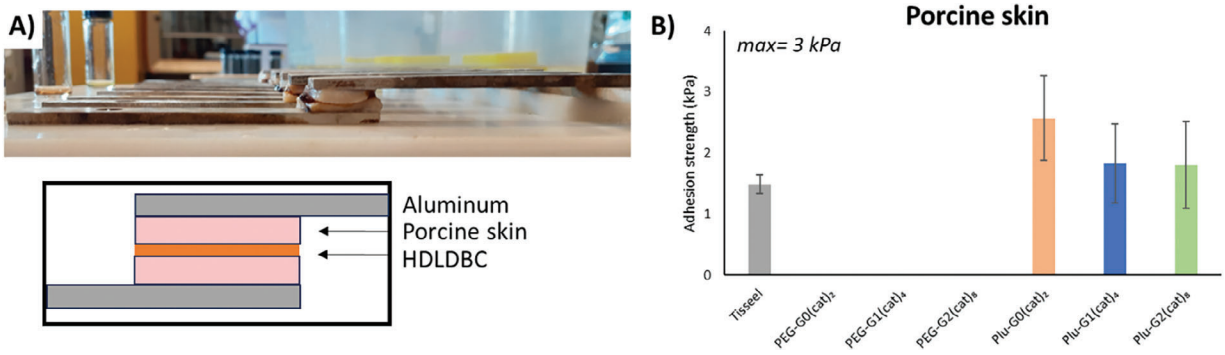

Figure 8. Bioadhesion. A) Picture of adhesion assay with porcine skin and B) Adhesion strength for PEG-based and Pluronic-based LDBCs on porcine skin after curing at 33 °C for 24 h. Sample size (n = 3). Numerical values are gathered in the Tables S10 (Supporting Information).

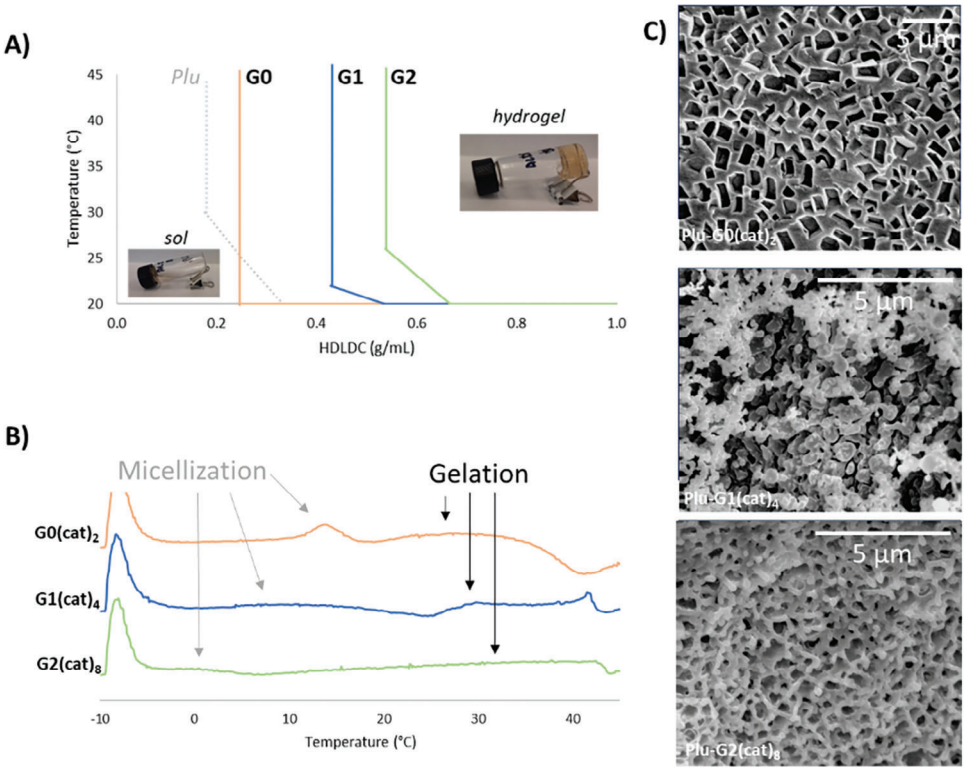

Figure 9. Pluronic-based LDBCs gelation in water. A) sol-gel phase diagrams of Pluronic LDBCs; B) derivatives of the DSC curves of the Pluronic-based LDBCs in water (C > CGC) and C) SEM images of the internal structure of the hydrogels formed by the Pluronic-based LDBCs.

starting at 0.25 g mL^{-1} for Plu-G0$(cat)_2$, 0.43 g mL^{-1} for Plu-G1$(cat)_4$ and 0.54 g mL^{-1} for Plu-G2$(cat)_8$. All of the CGCs were slightly higher than the one of unmodified Pluronic F-127, which was determined to be 0.18 g mL^{-1}. Hydrogelation was also detected by differential scanning calorimetry experiments in the thermograms of samples with concentration superior to the CGC (Figure 9B). New thermal events were observed in all cases at temperatures above the micellization peak, between 20 and 30 °C. SEM images of hydrogel samples prepared by freeze fracture revealed an internal porous structure with pores in the µm scale for Plu-G0$(cat)_2$ and Plu-G1$(cat)_4$, whereas Plu-G2$(cat)_8$ formed a more dense structure with pore sizes smaller than 1 µm. Accordingly, all the three Pluronic-based LDBCs, Plu-G0$(cat)_2$, Plu-G1$(cat)_4$ and Plu-G2$(cat)_8$, formed hydrogels under the conditions employed for adhesion tests on porcine skin (i.e., concentration of 0.8 g mL^{-1} and a curing temperature of 33 °C). Thanks to their self-assembling properties, all the three Pluronic-based LDBCs achieved effective bioadhesion. The dendritic structure did not induce a better adhesion in this case but resulted in hydrogels with different internal structures.

Overall, for bioadhesion, only the catechol-LDBCs based on Pluronic were able to show adhesion on porcine skin substrates with values similar to the commercial adhesive, TISSEEL. In this case, the self-assembly of the Pluronic-based LDBCs into macroscopic hydrogels fostered bioadhesion on skin. Such results lay the foundations for further investigations of catechol-LDBCs in bioadhesion.

3. Conclusion

In conclusion, two series of biomimetic catechol-functionalized LDBCs, based upon PEG or Pluronic F-127 for linear polymers and Bis-MPA derivatives as dendritic parts, were successfully synthesized. Like mussels, these LDBCs showed good adhesive properties. These linear-dendritic block copolymers could firmly stick aluminum substrates together with a maximum force tested of 7.6 MPa. Such a value is comparable to several commercial adhesives used on structural materials. Furthermore, a clear dendritic effect was observed in both series: PEG/Plu-G2$(cat)_8$ showed higher adhesion than PEG/Plu-G1$(cat)_4$, which, in turn, showed higher adhesion than PEG/Plu-G0$(cat)_2$. The dendritic architecture improved the adhesion of the linear polymers by concentrating locally the catechol moieties. Moreover, the catechol-LDBCs based on Pluronic were able to stick porcine skin, with adhesive values slightly higher than the commercial bioadhesive TISSEEL. Finally, a difference in adhesion was observed between the PEG and Pluronic series. The PEG-based catechol-LDBCs showed the highest adhesion on aluminum substrates, whereas only Pluronic-based catechol-LDBCs showed adhesion on porcine skin. This result was attributed to the self-assembly properties of Pluronic derivatives: the formation of micelles appeared to be detrimental for adhesion on aluminum whereas it was decisive for adhesion on porcine skin, thanks to the formation of hydrogels.

These results revealed the potential of developing catechol-containing linear-dendritic block copolymers for adhesion. The

dendritic architecture provided proper adhesion strength while the linear polymer structure allowed simplification of synthesis, purification and versatility. Such outcomes may have interesting implications for the future development of new adhesives to answer current challenges in bioadhesion.

4. Experimental Section

Materials: All reagents, including Pluronic F-127 and poly(ethylene glycol) (PEG) 10000, and dry solvents were purchased from Sigma–Aldrich and used without further purification. Non-dry solvents and Celite 541 were purchased from Fisher Scientific.

Aluminum 6061 ($8.9 \times 1.2 \times 0.3$ cm^3) was purchased from McMaster-Carr and used as a substrate material for adhesion experiments. Substrates were pre-treated by etching according to the ASTM D2651 standard method consisting in consecutive washes in base, acid, methanol and deionized water bathes.

Fresh porcine skin (15.2×15.2 cm^2) was purchased from Animal Technologies. It was collected from U.S. Department of Agriculture (USDA) certified or equivalent facilities, where animals receive ante mortem inspection and were found free of contagious disease. Hair, fat and subcutaneous tissue were removed. 1.2×1.2 cm^2 wet samples were glued onto aluminum 6061 substrates ($8.9 \times 1.2 \times 0.3$ cm^3) using a commercial 2-ethyl cyanoacrylate glue. They were placed in an incubating box at 33 °C with controlled humidity by placing a layer of 2 cm of water at the bottom of the box for 30 min prior the assay.

Synthesis: PEG-G1(OH)$_4$, PEG-G2(OH)$_8$, Plu-G1(OH)$_4$, and Plu-G2(OH)$_8$ were synthesized following previously published reports.[42,43] See Supporting Information-1: Synthesis for the detailed synthetic protocols and extended characterization.

Chemical Procedure for Activation with p-nitrophenyl chloroformate: In a round-bottom flask, the LDBC was dissolved into dry dichloromethane (c = 0.16 g mL^{-1}) by stirring over argon atmosphere. Then, dry pyridine (4.4 mol eq. per —OH group) was added to the LDBC solution. Room-temperature heated p-nitrophenyl chloroformate (4.0 mol eq. per —OH group) was added to the reaction mixture scoop by scoop. It was allowed to be stirred at room temperature for 24–48 h under argon atmosphere. After, the mixture was poured into cold diethyl ether (50 mL of diethyl ether/g of LDBC, −18 °C). The solid was recovered by centrifugation (12 000 rpm, 7 min, 4 °C) and was washed once with cold diethyl ether. This solid was then dissolved in ethyl acetate at 40 °C (20 mL of ethyl acetate/g of HDLBC) obtaining a mixture of solid and liquid. They were separated by centrifugation (12 000 rpm, 7 min, 40 °C). After the centrifugation, the white salt was disposed, and the supernatant was poured into cold diethyl ether (50 mL of diethyl ether/g of LDBC, −18 °C). The solid was recovered by centrifugation (12 000 rpm, 7 min, 4 °C) and was washed once with cold diethyl ether. The white solid was dried overnight in the fume hood.

See Supporting Information-1.2: Chemical characterization to see the LDBCs chemical structure and the proton labelling. PEG-G0(act)$_2$. ^{1}H NMR ($CDCl_3$, 400 MHz) δ (ppm): [3.44-3.73] (m, ≈900H, H-1,2), 3.78 (m, 4H, H-3), 4.41 (m, 4H, H-4), 7.37 (m, 4H, H-7), 8.25 (m, 4H, H-8). Remaining pyridine salt signals can be observed at 7.68, 7.29, and 8.62 ppm.

PEG-G1(act)$_4$. ^{1}H NMR ($CDCl_3$, 400 MHz) δ (ppm): 1.38 (s, 6H, H-7), [3.44-3.73] (m, ≈900H, H-1,2), 3.71 (m, 4H, H-3), 3.80 (m, 4H, H-4), 4.52 (ABq, J_{AB} = 11.0 Hz, $\Delta\nu_{AB}$ = 31.3 Hz, 8H, H-8), 7.36 (m, 4H, H-11), 8.25 (m, 8H, H-12). Remaining pyridine salt signals can be observed at 7.68, 7.29, and 8.62 ppm.

PEG-G2(act)$_8$. ^{1}H NMR ($CDCl_3$, 400 MHz) δ (ppm): 1.33 (s, 6H, H-7), 1.35 (s, 12H, H-11), [3.44-3.73] (m, ≈900H, H-1,2), 3.79 (m, 4H, H-3), 4.26 (m, 4H, H-4), 4.38 (ABq, J_{AB} = 11.2 Hz, $\Delta\nu_{AB}$ = 8.0 Hz, 8H, H-8), 4.45 (m, 16H, H-12), 7.36 (m, 16H, H-15), 8.24 (m, 16H, H-16). Remaining pyridine salt signals can be observed at 7.68, 7.29, and 8.62 ppm.

Plu-G0(act)$_2$. ^{1}H NMR ($CDCl_3$, 400 MHz) δ (ppm): 1.13 (m, 201H, H-1), 3.39 (m, 67H, H-2), [3.44-3.73] (m, ≈1000H, H-3,4,5), 3.81 (m, 4H, H-6), 4.43 (m, 4H, H-7), 7.39 (m, 4H, H-10), 8.27 (m, 4H, H-11). Remaining pyridine signals can be observed at 7.68, 7.29, and 8.62 ppm.

Plu-G1(act)$_4$. ^{1}H NMR ($CDCl_3$, 400 MHz) δ (ppm): 1.12 (m, 201H, H-1), 1.39 (s, 6H, H-10), 3.39 (m, 67H, H-2), [3.44-3.73] (m, ≈1000H, H-3,4,5), 3.80 (m, 4H, H-6), 4.35 (m, 4H, H-7), 4.53 (ABq, J_{AB} = 11.0 Hz, $\Delta\nu_{AB}$ = 42.3 Hz, 8H, H-11), 7.37 (m, 8H, H-14), 8.26 (m, 8H, H-15). Remaining pyridine signals can be observed at 7.68, 7.29, and 8.62 ppm.

Plu-G2(act)$_8$. ^{1}H NMR ($CDCl_3$, 400 MHz) δ (ppm): 1.11 (m, 201H, H-1), 1.32 (s, 6H, H-10), 1.35 (s, 12H, H-14), 3.37 (m, 67H, H-2), [3.42-3.13] (m, ≈1000H, H-3,4,5), 3.79 (m, 4H, H-6), 4.25 (m, 4H, H-7), 4.38 (ABq, J_{AB} = 11.1 Hz, $\Delta\nu_{AB}$ = 8.1 Hz, 8H, H-11), 4.45 (m, 16H, H-15), 7.36 (m, 16H, H-18), 8.23 (m, 16H, H-19). Remaining pyridine signals can be observed at 7.68, 7.29, and 8.62 ppm.

Chemical Procedure for Reaction with Dopamine: In a first round-bottom flask, the activated p-nitrophenyl chloroformate LDBC was dissolved into dry acetonitrile (c = 0.20 g mL^{-1}) by stirring over argon atmosphere at 45 °C. The solution was degassed with argon for 10 min. In a second round-bottom flask, dopamine hydrochloride (4.0 mol eq. per p-nitrophenol group) was dissolved into a mixture of dry dimethyl sulfoxide and dry pyridine (DMSO/Pyridine: 7/3, c = 0.15 g mL^{-1}). The dopamine solution was stirred under argon and degassed with argon for 10 min. Then, the degassed dopamine solution was added to the LDBC dissolution. The reaction mixture was degassed for 10 min with argon and the reaction mixture was allowed to stir under argon atmosphere at 45 °C for 48 h. After, the mixture was poured into a mixture of cold diethyl ether and cold ethanol (Et_2O/EtOH: 3/1, 50 mL of solvent/g of LDBC, −18 °C). The solid was recovered by centrifugation (12 000 rpm, 7 min, −5 °C) and was washed once with a mixture of cold diethyl ether and cold ethanol (Et_2O/EtOH: 3/1, −18 °C). Next, the solid was dissolved in dichloromethane (c = 0.05 g mL^{-1}) and stirred for 10 min obtaining a mixture of solid and liquid. They were separated by centrifugation (12 000 rpm, 7 min, 40 °C). After the centrifugation, the off-white solid was disposed, and the supernatant was poured into a mixture of cold diethyl ether and cold ethanol (Et_2O/EtOH: 3/1, 50 mL of solvent/g of LDBC, −18 °C). The solid was recovered by centrifugation (12 000 rpm, 7 min, −5 °C) and was washed once with a mixture of cold diethyl ether and cold ethanol (Et_2O/EtOH: 3/1). This solid was then dissolved in a small amount of dichloromethane and precipitated into a mixture of cold diethyl ether (50 mL of solvent/g of LDBC, −18 °C). The solid was recovered by centrifugation (12 000 rpm, 7 min, 4 °C) and was washed once with cold diethyl ether. The pale-yellow solid was dried overnight in the fume hood.

See Supporting Information-1.2: Chemical characterization to see the LDBCs chemical structure and the proton labelling. PEG-G0(cat)$_2$. ^{1}H NMR (CD_3CN, 400 MHz) δ (ppm): 2.61 (t, J = 7.4 Hz, 4H, H- 7), 3.42 (m, 4H, H-6), [3.44-3.73] (m, ≈900H, H-1,2,3), 4.09 (m, 4H, H-4), 5.52 (bs, ∼NH), 6.54 (dd, J = 8.0 Hz, J = 2.1 Hz, 2H, H-9), 6.66 (d, J = 2.1 Hz, 2H, H-13), 6.72 (d, J = 8.0 Hz, 2H, H-10), 7.23 (bs, ∼OH), 7.31 (bs, ∼OH). FT-IR (ν_{max}/cm^{-1}): ≈3500 (bs, O-H st), 2879 (C-H st), 1737 (C = O st), 1466 (CH_2, CH_3 δ), 1099 (C-O-C st). MS (MALDI$^+$): distribution with max at m/z 11320.

PEG-G1(cat)$_4$. ^{1}H NMR (CD_3CN, 400 MHz) δ (ppm): 1.18 (m, 6H, H-7), 2.61 (t, J = 7.0 Hz, 8H, H- 10), 3.22 (m, 8H, H-11), [3.44-3.73] (m, ≈900H, H-1,2,3), 4.12 (m, 8H, H-8), 4.19 (m, 4H, H-4), 5.68 (bs, ∼NH), 6.54 (dd, J = 8.0 Hz, J = 2.1 Hz, 4H, H-13), 6.64 (m, 4H, H-17), 6.72 (d, J = 8.0 Hz, 4H, H-14), 6.98 (bs, ∼OH), 7.07 (bs, ∼OH). FT-IR (ν_{max}/cm^{-1}): ∼3500 (bs, O-H st), 2880 (C-H st), 1737 (C = O st), 1466 (CH_2, CH_3 δ), 1099 (C-O-C st). MS (MALDI$^+$): distribution with max at m/z 12001.

PEG-G2(cat)$_8$. ^{1}H NMR (CD_3CN, 400 MHz) δ (ppm): 1.17 (m, 18H, H-7,11), 2.60 (t, 16H, H-15), 3.22 (m, 16H, H-14), [3.44-3.73] (m, ≈900H, H-1,2,3), 4.10 (m, 8H, H-8), 4.20 (m, 20H, H-4,12), 5.76 (bs, ∼NH), 6.53 (dd, J = 8.0 Hz, J = 2.1 Hz, 8H, H-17), 6.65 (m, 8H, H-21), 6.72 (d, J = 8.0 Hz, 8H, H-18), 6.91 (bs, ∼OH), 7.08 (bs, ∼OH). FT-IR (ν_{max}/cm^{-1}): ≈3300 (bs, O-H st), 2880 (C-H st), 1719 (C = O st), 1466 (CH_2, CH_3 δ), 1099 (C-O-C st). MS (MALDI$^+$): distribution with max at m/z 12920.

Plu-G0(cat)$_2$. ^{1}H NMR (CD_3CN, 400 MHz) δ (ppm): 1.07 (m, 201H, H-1), 2.61 (t, J = 7.4 Hz, 4H, H-10), 3.25 (m, 4H, H-9), 3.38 (m, 69H, H-2), [3.44-3.73] (m, ≈1000H, H-3,4,5,6), 4.09 (m, 4H, H-7), 5.53 (bs, ∼NH), 6.54 (dd, J = 8.0 Hz, J = 2.1 Hz, 2H, H-16), 6.66 (d, J = 2.1 Hz, 2H, H-12), 6.72 (d, J = 8.0 Hz, 2H, H-15), 7.01 (bs, ∼OH). FT-IR (ν_{max}/cm^{-1}): ≈3500

(bs, O-H st), 2864 (C-H st), 1718 (C = O st), 1466 (CH_2, CH_3 δ), 1093 (C-O-C st). MS ($MALDI^+$): distribution with max at m/z 13287.

Plu-G1(cat)$_4$. ^{1}H NMR (CD_3CN, 400 MHz) δ (ppm): 1.08 (m, 207H, H-1,10), 2.60 (t, J = 7.4 Hz, 4H, H-14), 3.23 (m, 4H, H-13), 3.38 (m, 69H, H-2), [3.44-3.73] (m, ≈1000H, H-3,4,5,6), 4.12 (m, 8H, H-11), 4.19 (m, 4H, H-7), 5.69 (bs, ∼NH), 6.55 (dd, J = 8.0 Hz, J = 2.1 Hz, 2H, H-20), 6.64 (d, J = 2.1 Hz, 2H, H-16), 6.72 (d, J = 8.0 Hz, 2H, H-19), 7.04 (bs, ∼OH). FT-IR (ν_{max}/cm^{-1}): ≈3500 (bs, O-H st), 2881 (C-H st), 1727 (C = O st), 1466 (CH_2, CH_3 δ), 1095 (C-O-C st). MS ($MALDI^+$): distribution with max at m/z 13645.

Plu-G2(cat)$_8$. ^{1}H NMR (CD_3CN, 400 MHz) δ (ppm): 1.07 (m, 201H, H-1), 1.17 (m, 18H, H-10,14), 2.60 (t, 16H, H-18), 3.22 (m, 16H, H-17), 3.39 (m, 69H, H-2), [3.44-3.73] (m, ≈1000H, H-3,4,5,6), 4.10 (m, 8H, H-11), 4.20 (m, 20H, H-7,15), 5.76 (bs, ∼NH), 6.53 (dd, J = 8.0 Hz, J = 2.1 Hz, 8H, H-24), 6.66 (m, 8H, H-20), 6.72 (d, J = 8.0 Hz, 8H, H-23), 6.93 (bs, ∼OH), 7.18 (bs, ∼OH). FT-IR (ν_{max}/cm^{-1}): ≈3500 (bs, O-H st), 2864 (C-H st), 1726 (C = O st), 1466 (CH_2, CH_3 δ), 1097 (C-O-C st). MS ($MALDI^+$): distribution with max at m/z 13710.

Chemical Characterization: The ^{1}H nuclear magnetic resonance (^{1}H NMR) spectra were registered using a Bruker AV-III-400-HD NMR equipped with a 5 mm BBFO Z-gradient SmartProbe. The spectra were recorded at 400 MHz employing deuterated chloroform or deuterated acetonitrile for solvent. The chemical shifts were given in ppm relative to tetramethylsilane and the coupling constant in Hz. The solvent residual peak was used for an internal standard. The Fourier transform Infrared (FTIR) spectra were collected using a Thermo Nicolet Nexus FT-IR in attenuated total reflectance mode using a ZnSe probe and were recorded from 4000 to 850 cm^{-1}. The $MALDI^+$ spectra were collected using a Voyager DE-Pro MALDI-TOF Mass Spectrometer with runs in the 5–25 kDa range in linear positive and reflector positive. SEC traces were collected using a Walter e2695 Alliance employing two in series HR4 and HR1 Styragel columns and a light scattering detector at a flow rate of 1 mL min^{-1} at 35 °C. Tetrahydrofuran was used as a solvent and the samples were injected at the concentration of 1 mg mL^{-1}.

Waite and Benedict DOPA Assay (with UV–vis) for Catechol Containing Determination: Each LDBC (m = 10–30 mg) was dissolved in distilled water (V = 1 mL) and placed at 4 °C overnight to ensure the full dissolution of the LDBCs. Next, 100 µL of each LDBC solution were added to 900 µL of HCl 1 M. Then, 900 µL of a solution of $NaNO_2$ 1.45 M and $NaMbO_4$ 0.41 M were added to each solution and immediately followed by the addition of 1600 µL of NaOH 1 M. Then, the UV–vis absorbance of each solution was measured at λ = 500 nm after 3 min using a Varian Cary 100 Bio UV–vis apparatus. The measured absorbance was compared to a standard curve obtained using known concentrations of dopamine hydrochloride in water (Figure S9, Supporting Information).

Red Nile Assay (with Fluorimeter) for Micellization Assay and Critical Micellization Concentration (CMC) Determination: Each LDBC was dissolved in distilled water (c = 100 mg mL^{-1}, V = 1 mL). The solutions were placed at 4 °C overnight to ensure the full dissolution of the LDBCs. 10 µL of a Red Nile solution (c = 3.18 mg mL^{-1} in ethanol) were added to each solution. The resulting solutions were stirred in dark for 1 h at 20 °C. The emission fluorescence spectrum was recorded for each solution (λ_{ext} = 550 nm, λ_{em} = 570 to 750 nm) using an Edinburgh Instruments FLS980 Fluorometer at 20 °C. To determine the CMC of the Pluronic-based LDBCs at 20 °C, the same protocol was followed using LDBC solutions with LDBCs concentrations ranging from 2 to 100 mg mL^{-1}.

Viscosity Measurement: PEG-G2(cat)$_8$ and Plu-G2(cat)$_8$ were dissolved in water at 0.48 g mL^{-1}. The solutions were placed at 4 °C to ensure the full dissolution of the LDBCs. The stock solution of each LDBCs was further diluted in order to obtain additional dissolutions at 0.36, 0.24, and 0.12 g mL^{-1} in water. The viscosity of each dissolution was measured on a HAAKE MARS 40 rheometer equipped with a cone and plate geometry (cone diameter 35 mm, 1° inclination) and a Peltier module for temperature control. 300 µL of LDBC solution were transferred on the plate and the gap was set to 0.047 mm. Excess solution was trimmed off and a thin layer of silicone oil was added to prevent evaporation. Samples were stabilized in the measuring geometry for 10 min at 20 °C. Measurements were conducted in the 1 to 100 1/s range recording six data points every decade.

Sol-Gel Phase Diagram Determination Using the Vial Inversion Technique: Pluronic F-127 and the Pluronic-based LDBCs were dissolved within transparent glass vials at the following concentrations: 0.11, 0.18. 0.25, 0.33, 0.43, 0.54, 0.66, 0.82, and 1.00 g mL^{-1} (V = 1 mL). The samples were placed at 4 °C overnight to ensure the full dissolution of the LDBCs. The samples that remained heterogeneous after that time were placed 1 h at −18 °C. After, the samples were heated from 20 to 44 °C using 2 °C steps by means of a water bath. After reaching each step, the physical state of the samples (sol or gel) was determined using the vial inversion technique after waiting for 5 min to let the sample reach an equilibrium.

Differential Scanning Calorimetry (DSC) of the Aqueous Solutions: Each LDBC was dissolved in distilled water (V = 0.5 mL) at the following concentrations: for PEG-G0(cat)$_2$, PEG-G1(cat)$_4$ and PEG-G2(cat)$_8$, c = 0.30 mg mL^{-1}, for Plu-G0(cat)$_2$, c = 0.15 g mL^{-1} (<CGC) and c = 0.30 mg mL^{-1} (>CGC), and for Plu-G1(cat)$_4$ and Plu-G2(cat)$_8$, c = 0.30 g mL^{-1} (<CGC) and c = 0.60 mg mL^{-1} (>CGC). The solutions were placed at 4 °C overnight to ensure the full dissolution of the LDBCs. 15–20 mg of each solution were placed in a non-sealed aluminum pan. The measurements were performed using a Perkin Elmer DSC 4000 and collected during a 5 °C min^{-1} heating ramp from −10 to 50 °C.

Scanning Electron Microscopy (SEM): For the micelles observation, Plu-G0(cat)$_2$ was dissolved in water (V = 100 µL) at 0.1 g mL^{-1}. The solutions were placed at 4 °C overnight to ensure the full dissolution of the LDBCs. A drop of solution was placed on SEM sample holder and the solvent was evaporated at room temperature for 24 h. The sample was coated with platinum. Images were collected using a FEI Quanta 3D FEG instrument. For the hydrogel observation, Plu-G0(cat)$_2$, Plu-G1(cat)$_4$ and Plu-G2(cat)$_8$ were mixed in water (V = 50 µL) at 0.8 g mL^{-1}. The solutions were placed at 4 °C for 1 h, followed by 1 h at −18 °C and overnight at 4 °C to ensure the homogeneous formation of the hydrogel. The hydrogels were frozen at −196 °C using liquid nitrogen. A small part of the frozen hydrogel was placed on a SEM sample holder. It was placed in a cryochamber where it was cut and then coated with platinum. Images were collected using a FEI Cryogenic Dual Beam-Nova instrument.

Cryogenic Transmission Electron Microscopy (cryo-TEM): Plu-G0(cat)$_2$, Plu-G1(cat)$_4$ and Plu-G2(cat)$_8$ were dissolved in water (V = 100 µL) at 0.1 g mL^{-1}. The solutions were placed at 4 °C overnight to ensure the full dissolution of the LDBCs. The solution was diluted ten times just before its application onto the TEM grid to avoid grid saturation with sample. Then, 20 µL of this solution were placed on previously UV-ionized TEM grid. The sample vitrification was performed using a vitrobot and using liquid ethane. Images were collected using a FEI TECNAI T20.

Lap Shear Adhesion Assays on Aluminum (with Instron 5544 Material Testing System): For the concentration study, each LDBC was dissolved in distilled water (c = 0.06–0.48 mg mL^{-1}, V = 0.5 mL). The solutions were placed at 4 °C overnight to ensure the full dissolution of the LDBCs. Then, 30 µL of each solution were deposited onto one substrate and 15 µL onto the other substrate using a positive displacement pipette. The substrates were overlapped to form a single lap shear joint (1.2 × 1.2 cm^2). Two clips were used to firmly block the joint.

For the $Fe^{(III)}$ crosslinking study, each LDBC was dissolved in distilled water (c = 0.3 mg mL^{-1}, V = 0.5 mL) together with $FeCl_3 \cdot 6H_2O$. The solutions were placed at 4 °C overnight to ensure the full dissolution of the LDBCs and promote crosslinking. Then, 30 µL of each solution were deposited onto one substrate and 15 µL onto the other substrate using a positive displacement pipette. The substrates were overlapped to form a single lap shear joint (1.2 × 1.2 cm^2). Two clips were used to firmly block the joint.

All the samples were cured for 1 h at room temperature, followed by 22 h at 120 °C and then 1 h at room temperature. Lap shear adhesion forces were measured using a Instron 5544 materials testing system. The substrates were pulled apart at a rate of 2 mm min^{-1} until the adhesive failed. The maximum force (in N) required to break the joint was divided by the overlapping surface area (in m^2) to give the adhesion strength (in Pa). Each adhesion experiment was performed with five samples and data were averaged. Error bars correspond to the standard deviation.

Adhesion assays with Gorilla glue and Super Glue for benchmarking were performed in the same conditions except for curing that was carried

out for 24 h at room temperature following the manufacturer's recommendations.

Lap Shear Adhesion Assays on Porcine Skin (with Instron 5544 Material Testing System): Each LDBC was dissolved in distilled water (c = 0.8 g mL^{-1}, V = 0.3 mL). The solutions were placed at 4 °C overnight to ensure the full dissolution of the LDBCs. After, 40 µL of each solution were deposited onto one substrate and 40 µL onto the other substrate using a positive displacement pipette. The substrates were overlapped to form a single lap shear joint (1.2 × 1.2 cm^2) and a 50 g weight were placed on top of the joint. The samples were cured for 24 h at 33 °C.

Lap shear adhesion forces were measured using a Instron 5544 materials testing system. The substrates were pulled apart at a rate of 2 mm min^{-1} until the adhesive failed. The maximum force (in N) required to break the joint was divided by the overlapping surface area (in m^2) to give the adhesion strength (in Pa). Each adhesion experiment was performed with three samples and data were averaged. Error bars correspond to the standard deviation.

Adhesion assays with TISSEEL for benchmarking were performed in the same conditions.

Statistical Analysis—Pre-Processing of Data: Recorded ^{1}H NMR signals were processed using Fourier transformation and the phase was automatically corrected. Recorded FTIR signals were processed using Fourier transformation. Recorded SEC traces were normalized and the integration of the area under the curve to determine the relative molecular weight and the polydispersity were manually performed. The areas under the curve (in N.mm) obtained during the adhesion assays were automatically calculated.

Statistical Analysis—Data Presentation and Sample Size: Aluminum lap shear adhesion assays were performed with five samples and data were averaged. Porcine skin lap shear adhesion assays were performed with three samples and data were averaged. In all cases, results were presented as mean ± SD. In every bar graph, the bar represents the mean value, and the error bar represents the standard deviation.

Supporting Information

Supporting Information is available from the Wiley Online Library or from the author.

Acknowledgements

The authors appreciate the support for this project provided by the European Commission through the Marie Skłodowska-Curie Actions (MSCA) fundings – Horizon Europe, Grant no. 101062504 – DAHAD project. The authors thank the Office of Naval Research (Award N00014-19-1-2342). This work was financially supported by the Spanish projects PID2021-126132NB-I00, financed by MCIU/AEI/10.13039/501100011033/ and by "ERDF A way of making Europe", and CEX2023-001286-S, financed by MCIU/AEI/10.13039/501100011033/, and the Gobierno de Aragón-FEDER (E47_23R-research group). The authors would like to acknowledge the Laboratorio de Microscopias Avanzadas-LMA (Instituto de Nanociencia y Materiales de Aragón-Universidad de Zaragoza). We acknowledge support of the publication fee by the CSIC Open Access Publication Support Initiative through its Unit of Information Resources for Research (URICI).

Conflict of Interest

JJW has a financial stake in a startup company, Mussel Polymers Inc., which is commercializing catechol-based adhesives. The polymers in development at the company revolve around poly(vinylcatechol-styrene) and are distinct from the PEG- and Pluronic-based systems described in this paper.

Data Availability Statement

The data that support the findings of this study are available from the corresponding author upon reasonable request.

Keywords

biomimetics, block copolymers, dendrimers, gelation, micellization, skin adhesion

Received: July 25, 2024
Revised: September 4, 2024
Published online:

[1] Q. Lin, D. Gourdon, C. Sun, N. Holten-Andersen, T. H. Anderson, J. H. Waite, J. N. Israelachvili, *Proc. Natl. Acad. Sci. USA* **2007**, *104*, 3782.
[2] Q. Lu, E. Danner, J. H. Waite, J. N. Israelachvili, H. Zeng, D. S. Hwang, *J. Royal Soc. Interface* **2013**, *10*, 20120759.
[3] E. W. Danner, Y. Kan, M. U. Hammer, J. N. Israelachvili, J. H. Waite, *Biochemistry* **2012**, *51*, 6511.
[4] P. Kord Forooshani, B. P. Lee, *J. Polym. Sci. Part A Polym. Chem.* **2017**, *55*, 9.
[5] J. Saiz-Poseu, J. Mancebo-Aracil, F. Nador, F. Busqué, D. Ruiz-Molina, *Angew. Chemie – Int. Ed.* **2019**, *58*, 696.
[6] S. Xu, M. Kang, X. Xin, J. Liang, H. Xiao, Y. Lu, J. Yang, H. Zhai, *J. Environ. Chem. Eng.* **2024**, *12*, 111655.
[7] S. Seo, S. Das, P. J. Zalicki, R. Mirshafian, C. D. Eisenbach, J. N. Israelachvili, J. H. Waite, B. K. Ahn, *J. Am. Chem. Soc.* **2015**, *137*, 9214.
[8] C.-W. Chu, Y. Zhang, T. Kubo, S. Tanizaki, K. Kojio, K. Satoh, A. Takahara, *ACS Appl. Polym. Mater.* **2022**, *4*, 3687.
[9] H. J. Meredith, C. L. Jenkins, J. J. Wilker, *Adv. Funct. Mater.* **2014**, *24*, 3259.
[10] C. L. Jenkins, H. M. Siebert, J. J. Wilker, *Macromolecules* **2017**, *50*, 561.
[11] B. D. B. Tiu, P. Delparastan, M. R. Ney, M. Gerst, P. B. Messersmith, *Angew. Chemie – Int. Ed.* **2020**, *59*, 16616.
[12] Q. Guo, J. Chen, J. Wang, H. Zeng, J. Yu, *Nanoscale* **2020**, *12*, 1307.
[13] H. Fan, J. P. Gong, *Adv. Mater.* **2021**, *33*, 2102983.
[14] M. A. North, C. A. Del Grosso, J. J. Wilker, *ACS Appl. Mater. Interfaces* **2017**, *9*, 7866.
[15] A. Lancelot, A. A. Putnam-Neeb, S. L. Huntington, J. M. Garcia-Rodriguez, N. Naren, C. L. Atencio-Martinez, J. J. Wilker, *Macromolecules* **2023**, *56*, 1141.
[16] A. Li, Y. Mu, W. Jiang, X. Wan, *Chem. Commun.* **2015**, *51*, 9117.
[17] Y. Xu, Q. Liu, A. Narayanan, D. Jain, A. Dhinojwala, A. Joy, *Adv. Mater. Interfaces* **2017**, *4*, 1700506.
[18] B. Khasheii, P. Mahmoodi, A. Mohammadzadeh, *Microbiol. Res.* **2021**, *250*, 126790.
[19] E. Abbasi, S. F. Aval, A. Akbarzadeh, M. Milani, H. T. Nasrabadi, S. W. Joo, Y. Hanifehpour, K. Nejati-Koshki, R. Pashaei-Asl, *Nanoscale Res. Lett.* **2014**, *9*, 247.
[20] J. M. J. Fréchet, *Proc. Natl. Acad. Sci. USA* **2002**, *99*, 4782.
[21] M. Sowinska, Z. Urbanczyk-Lipkowska, *New J. Chem.* **2014**, *38*, 2168.
[22] M. A. Mintzer, E. L. Dane, G. A. O'Toole, M. W. Grinstaff, *Mol. Pharmaceutics* **2012**, *9*, 342.
[23] D. A. Tomalia, *New J. Chem.* **2012**, *36*, 264.
[24] A. M. Caminade, A. Ouali, R. Laurent, C. O. Turrin, J. P. Majoral, *Chem. Soc. Rev.* **2015**, *44*, 3890.
[25] H. F. Chow, C. F. Leung, G. X. Wang, Y. Y. Yang, *Comptes Rendus Chim.* **2003**, *6*, 735.
[26] J. Lee, W. T. Ford, J. A. Moore, Y. Li, *Macromolecules* **1994**, *27*, 4632.

[27] C. Valério, E. Alonso, J. Ruiz, J.-C. Blais, D. Astruc, *Angew. Chem., Int. Ed.* **1999**, *38*, 1747.
[28] E. M. Munoz, J. Correa, R. Riguera, E. Fernandez-Megia, *J. Am. Chem. Soc.* **2013**, *135*, 5966.
[29] L. P. Wu, M. Ficker, J. B. Christensen, D. Simberg, P. N. Trohopoulos, S. M. Moghimi, *Nat. Commun.* **2021**, *12*, 4858.
[30] Q. Wei, K. Achazi, H. Liebe, A. Schulz, P. L. M. Noeske, I. Grunwald, R. Haag, *Angew. Chemie – Int. Ed.* **2014**, *53*, 11650.
[31] A. Ghosh, J. Singh, S. Lim, T. W. J. Steele, *Mater. Today Adv.* **2023**, *19*, 100398.
[32] L. Gan, N. C. S. Tan, A. Gupta, M. Singh, O. Pokholenko, A. Ghosh, Z. Zhang, S. Li, T. W. J. Steele, *Chem. Commun.* **2019**, *55*, 10076.
[33] C. Cui, C. Fan, Y. Wu, M. Xiao, T. Wu, D. Zhang, X. Chen, B. Liu, Z. Xu, B. Qu, W. Liu, *Adv. Mater.* **2019**, *31*, 1905761.
[34] H. Zhu, G. Xu, Y. He, H. Mao, D. Kong, K. Luo, W. Tang, R. Liu, Z. Gu, *Adv. Healthcare Mater.* **2022**, *11*, 2200874.
[35] N. Sanz del Olmo, N. Molina, Y. Fan, F. Namata, D. J. Hutchinson, M. Malkoch, *J. Am. Chem. Soc.* **2024**, *146*, 17240.
[36] M. J. Poellmann, K. Javius-Jones, C. Hopkins, J. W. Lee, S. Hong, *Bioconjug. Chem.* **2022**, *33*, 2008.
[37] C. E. Brubaker, P. B. Messersmith, *Biomacromolecules* **2011**, *12*, 4326.
[38] J. Feng, X. A. Ton, S. Zhao, J. I. Paez, A. del Campo, *Biomimetics* **2017**, *2*, 23.
[39] Y. Lee, H. J. Chung, S. Yeo, C. H. Ahn, H. Lee, P. B. Messersmith, T. G. Park, *Soft Matter* **2010**, *6*, 977.
[40] L. Almásy, O. P. Artykulnyi, V. I. Petrenko, O. I. Ivankov, L. A. Bulavin, M. Yan, V. M. Haramus, *Molecules* **2022**, *27*, 2573.
[41] A. Naharros-Molinero, M. Á. Caballo-González, F. J. de la Mata, S. García-Gallego, *Pharmaceutics* **2022**, *14*, 2628.
[42] H. Ihre, O. L. Padilla De Jesús, J. M. J. Fréchet, *J. Am. Chem. Soc.* **2001**, *123*, 5908.
[43] I. Jiménez-Pardo, R. González-Pastor, A. Lancelot, R. Claveria-Gimeno, A. Velázquez-Campoy, O. Abian, M. B. Ros, T. Sierra, *Macromol. Biosci.* **2015**, *15*, 1381.
[44] J. H. Waite, C. V. B. T.-M. E. Benedict, In *Posttranslational Modifications Part B*, Academic Press, Cambridge, Massachusetts **1984**.
[45] E. Martí Coma-Cros, A. Lancelot, M. San Anselmo, L. Neves Borgheti-Cardoso, J. J. Valle-Delgado, J. L. Serrano, X. Fernàndez-Busquets, T. Sierra, *Biomater. Sci.* **2019**, *7*, 1661.
[46] A. J. Kinloch, *Adhesion and Adhesives: Science and Technology*, Chapman and Hall, London **1987**.
[47] S. Lowe, N. M. O'Brien-Simpson, L. A. Connal, *Polym. Chem.* **2015**, *6*, 198.
[48] J. Bizeau, A. Adam, S. Bégin-Colin, D. Mertz, *Eur. J. Inorg. Chem.* **2021**, *2021*, 4799.
[49] B. Cheng, J. Yu, T. Arisawa, K. Hayashi, J. J. Richardson, Y. Shibuta, H. Ejima, *Nat. Commun.* **2022**, *13*, 1892.
[50] Z. D. Lamberty, N. T. Tran, C. D. van Engers, P. Karnal, D. B. Knorr, J. Frechette, *ACS Appl. Mater. Interfaces* **2023**, *15*, 35720.
[51] G. Wanka, H. Hoffmann, W. Ulbricht, *Macromolecules* **1994**, *27*, 4145.
[52] E. Martí Coma-Cros, A. Lancelot, M. San Anselmo, L. Neves Borgheti-Cardoso, J. J. Valle-Delgado, J. L. Serrano, X. Fernàndez-Busquets, T. Sierra, *Biomater. Sci.* **2019**, *7*, 1661.
[53] Z. Gu, M. Wang, Q. Fang, H. Zheng, F. Wu, D. Lin, Y. Xu, Y. Jin, *Drug Dev. Ind. Pharm.* **2015**, *41*, 812.
[54] M. C. A. Stuart, J. C. Van De Pas, J. B. F. N. Engberts, *J. Phys. Org. Chem.* **2005**, *18*, 929.
[55] A. Cabana, A. Aït-Kadi, J. Juhász, *J. Colloid Interface Sci.* **1997**, *190*, 307.
[56] Y. Li, J. Wen, M. Qin, Y. Cao, H. Ma, W. Wang, *ACS Biomater. Sci. Eng.* **2017**, *3*, 979.
[57] J. Bijlsma, W. J. C. de Bruijn, J. A. Hageman, P. Goos, K. P. Velikov, J. P. Vincken, *Sci. Rep.* **2020**, *10*, 8288.
[58] X. Fan, Y. Zhao, W. Xu, L. Li, *Mater. Sci. Eng. C* **2016**, *62*, 943.
[59] N. Feliu, M. V. Walter, M. I. Montañez, A. Kunzmann, A. Hult, A. Nyström, M. Malkoch, B. Fadeel, *Biomaterials* **2012**, *33*, 1970.
[60] Y. Hed, Y. Zhang, O. C. J. Andrén, X. Zeng, A. M. Nyström, M. Malkoch, *J. Polym. Sci. Part A Polym. Chem.* **2013**, *51*, 3992.
[61] J. Movellan, P. Urbán, E. Moles, J. M. de la Fuente, T. Sierra, J. L. Serrano, X. Fernàndez-Busquets, *Biomaterials* **2014**, *35*, 7940.